Long-Lived Triplet Excited State Accessed with Spin–Orbit Charge Transfer Intersystem Crossing in Red Light-Absorbing Phenoxazine-Styryl BODIPY Electron Donor/Acceptor Dyads

Yu Dong,[a] Ayhan Elmali,[b] Jianzhang Zhao,*[a] Bernhard Dick,*[c] and Ahmet Karatay*[b]

Orthogonal phenoxazine-styryl BODIPY compact electron donor/acceptor dyads were prepared as heavy atom-free triplet photosensitizers (PSs) with strong red light absorption ($\varepsilon = 1.33 \times 10^5$ M^{-1}cm^{-1} at 630 nm), whereas the previously reported triplet photosensitizers based on the spin-orbit charge transfer intersystem crossing (SOCT-ISC) mechanism show absorption in a shorter wavelength range (< 500 nm). More importantly, a long-lived triplet state ($\tau_T = 333$ μs) was observed for the new dyads. In comparison, the triplet state lifetime of the same chromophore accessed with the conventional heavy atom effect (HAE) is much shorter ($\tau_T = 1.8$ μs). Long triplet state lifetime is beneficial to enhance electron or energy transfer, the primary photophysical processes in the application of triplet PSs. Our approach is based on SOCT-ISC, without invoking of the HAE, which may shorten the triplet state lifetime. We used bisstyrylBodipy both as the electron acceptor and the visible light-harvesting chromophore, which shows red-light absorption. Femtosecond transient absorption spectra indicated the charge separation (109 ps) and SOCT-ISC (charge recombination, CR; 2.3 ns) for **BDP-1**. ISC efficiency of **BDP-1** was determined as $\Phi_T = 25\%$ (in toluene). The dyad **BDP-3** was used as triplet PS for triplet-triplet annihilation upconversion (upconversion quantum yield $\Phi_{UC} = 1.5\%$; anti-Stokes shift is 5900 cm^{-1}).

1. Introduction

Triplet photosensitizers (PSs) are compounds showing intersystem crossing (ISC) to populate triplet excited state upon photoexcitation. Much attention has been paid to the design of new triplet PSs and for their applications in photo-redox catalytic organic reactions,[1] photodynamic therapy (PDT),[2] H$_2$ production by photocatalytic water splitting,[3] triplet-triplet annihilation upconversion (TTA-UC),[4] and photovoltaics.[5] The triplet state production is via ISC, a spin forbidden non-radiative electronic transition. A traditional strategy of enhancing ISC is to introduce transition metal atoms such as Ru, Ir, Pt or other heavy atoms, such as I or Br.[6] However, drawbacks of this heavy atom effect (HAE) are the high cost of the synthesis, and the toxicity of the compounds. Moreover, the triplet state lifetime of these PSs is shortened since the HAE enhance not only the ISC of S$_1 \rightarrow$T$_n$, but also the T$_1 \rightarrow$S$_0$ ISC process.[7]

Charge recombination (CR)-induced ISC was known for electron donor/acceptor dyads with a long and rigid linker between donor and acceptor.[8] A large distance, thus a weak electronic coupling and a small electron exchange energy (J), is indispensable for the radical pair ISC (RP ISC) mechanism in these conventional electron donor/acceptor dyads. This type of ISC is based on the hyperfine interaction enhanced ^{1}CT$\rightarrow^3$CT process (CT: charge transfer), followed by ^{3}CT$\rightarrow$locally excited triplet state (^{3}LE) internal conversion (given the purpose is to access the ^{3}LE, not the long-lived CT state). However, these conventional electron donor/acceptor dyads are difficult to prepare, and generally the molecular structures are not optimized for triplet PS preparation, and the visible light-harvesting ability is poor. When the linker between the electron donor and acceptor was reduced in length, for instance by a direct link between donor and acceptor in compact dyads, the electronic coupling and the electron exchange energy increase, and RP ISC is inhibited.[9]

Recently, efficient ISC was observed for the CR in some compact electron donor/acceptor dyads via the so-called spin orbit charge transfer intersystem crossing (SOCT-ISC).[10] The ISC process requires conservation of the total angular momentum,

[a] Y. Dong, Prof. J. Zhao
     State Key Laboratory of Fine Chemicals
     School of Chemical Engineering
     Dalian University of Technology
     E-208 West Campus, 2 Ling Gong Road, Dalian 116024, China
     E-mail: zhaojzh@dlut.edu.cn
[b] Dr. A. Elmali, Dr. A. Karatay
     Department of Engineering Physics
     Faculty of Engineering
     Ankara University
     06100 Beşevler, Ankara, Turkey
     E-mail: Ahmet.Karatay@eng.ankara.edu.tr
[c] Prof. B. Dick
     Lehrstuhl für Physikalische Chemie
     Institut für Physikalische und Theoretische Chemie
     Universität Regensburg
     Universitätsstr. 31, 93053 Regensburg, Germany
     E-mail: Bernhard.Dick@chemie.uni-regensburg.de

ChemPhysChem

Articles
doi.org/10.1002/cphc.202000300

**Chemistry
Europe**
European Chemical
Societies Publishing

i.e. the sum of orbital angular momentum and spin angular momentum.[10] Given the electron donor and acceptor moieties in a dyad adopt orthogonal orientation, the change of molecular orbital angular momentum of the CR will offset the change of electron spin angular momentum of ISC.[10b] Therefore, conservation of angular momentum is satisfied in the ISC of an orthogonal electron donor-acceptor dyad. Hence the SOCT-ISC is efficient in orthogonal electron donor/acceptor dyad. It should be pointed out some electron donor/acceptor dyads undergo twisted intramolecular charge transfer (TICT) may also show the charge recombination induced ISC.

Advantages of these novel compact electron donor/acceptor dyads are their simple molecular structure and long triplet state lifetimes. These features are important for applications of triplet PSs in photocatalysis and PDT. Several chromophores have been used for preparation of electron donor/acceptor compact dyads showing SOCT-ISC, such as acridinium,[10a] anthracene,[10b] perylene,[12] BODIPY,[10c,13] and perylenemonoimide/perylenediimide,[14] etc. However, triplet PSs based on SOCT-ISC showing red light absorption were rarely reported.[15] In some cases, long-lived ^{3}CT state was observed for the compact dyad.[16] On the other hand, although BODIPY-derived triplet PSs showing red light absorption have been reported, for instance the 2,6-diiodostyrylBodipy,[17] and the 2,6-diiodoazaBodipy,[18] the triplet state lifetimes of these red light-absorbing triplet PSs are short (~1.8 μs), which is a clear disadvantage for the applications in PDT,[7b] TTA-UC,[4d,19] or

photocatalysis, etc.[20] In these applications, the intermolecular electron transfer or triplet energy transfer efficiency increases with longer triplet state lifetime of the PSs.

Inspired by the previous results, herein we selected styryl BODIPY as the electron acceptor and red-light-absorbing chromophore, and phenoxazine (PXZ) as the electron donor, in order to design compact, orthogonal electron donor/acceptor dyads as novel heavy atom-free triplet PSs showing red light-absorption and long-lived triplet states (Scheme 1). PXZ has been used in thermally activated delayed fluorescence materials (TADF),[21] and photovoltaics.[1a] Compared with the previously used phenothiazine (PTZ. oxidation potential $E_{OX} = +0.21$ V vs. Fc/Fc$^+$), PXZ has a more planar π-conjugated structure and different redox properties (oxidation potential $E_{OX} = +0.36$ V vs. Fc/Fc$^+$).[22] It may provide different solvent polarity-dependency for the SOCT-ISC. To obtain more PSs with red light-absorption, large π-conjugated carbazole moiety is attached at the 2,6-positions of BODIPY (**BDP-3**, Scheme 1), which may change the triplet state lifetime or triplet state energy, and finally the ISC efficiency.

The photophysical properties of the dyads were studied by steady-state and time-resolved transient spectroscopies. The CS and CR were studied with femtosecond transient absorption spectra, and the triplet state spectra and lifetimes were studied with nanosecond transient absorption spectra. The new heavy atom-free triplet PSs were used for TTA-UC, and larger anti-Stokes shift was achieved (0.68 eV) than the recently reported
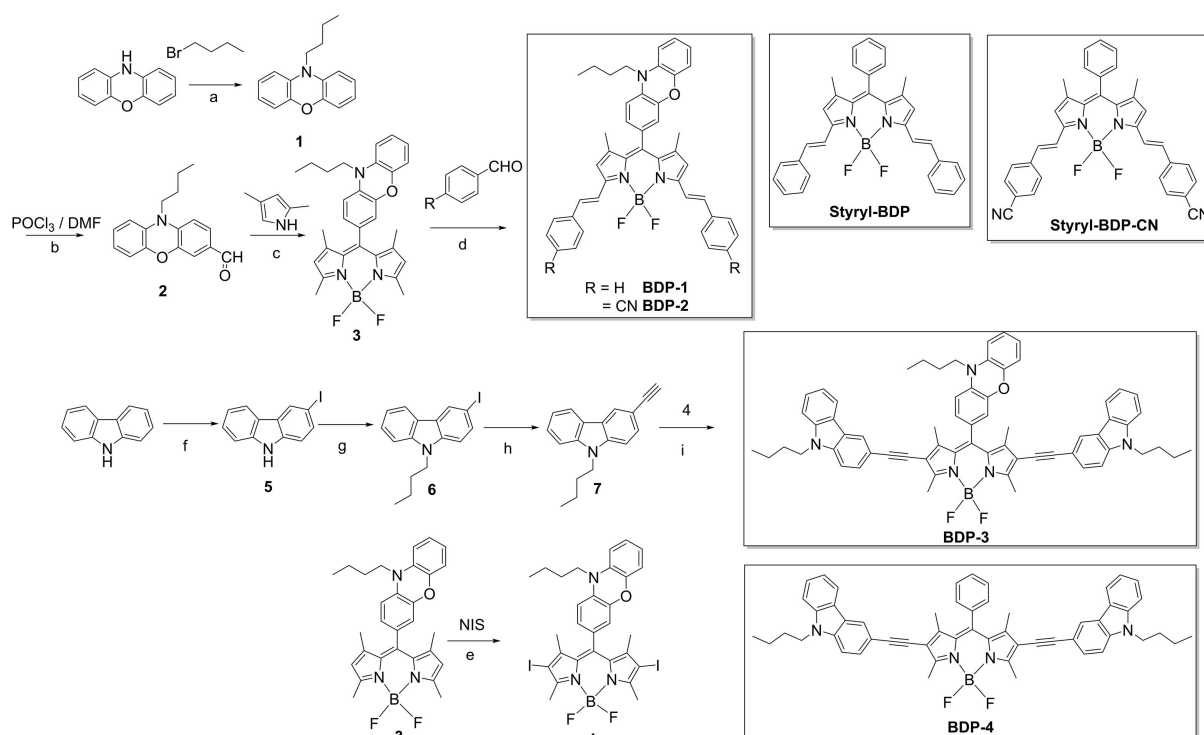
Scheme 1. Synthesis of the Compounds. a) n-C$_4$H$_9$Br, DMF, KOH, N$_2$, stirred at RT for 2 h, yield: 60%; b) POCl$_3$, DMF, N$_2$, 90 °C, 2 h, yield: 65%; c) 2,4-dimethylpyrrole, TFA, DDQ, TEA, BF$_3$·Et$_2$O, DCM, RT, N$_2$, yield: 6%; d) aryl aldehyde, p-toluenesulfonic acid, piperidine, 15 min, yield: 42% for R=H and 13% for R=CN; e) NIS, DCM, RT for 2 h, yield: 89%; f) KI, KIO$_3$, acetic acid, 85 °C, 10 min, 39%; g) n-C$_4$H$_9$Br, DMSO, NaH, N$_2$, stirred at RT for 2 h, yield: 90%; h) PdCl$_2$(PPh$_3$)$_2$, PPh$_3$, CuI, TEA, TMSA, N$_2$, 80 °C, 6 h; then stirred at RT over night, yield: 70%; i) PdCl$_2$(PPh$_3$)$_2$, PPh$_3$, CuI, TEA and THF, N$_2$, 65 °C, 2 h, yield: 60%.

PXZ-Bodipy dyads showing green light absorption (the anti-Stokes shift is *ca.* 0.36 eV).[22]

2. Results and Discussion

2.1. Molecular Structure Designing Rationales

Phenoxazine (PXZ) is used as electron donor. Styryl BODIPY is selected as electron acceptor and red-light-absorbing chromophore. The cyano groups attached to the styryl BODIPY moiety in **BDP-2** will enhance the electron withdrawing ability, which may produce a more efficient charge transfer. The PXZ moiety was attached at the 8-position (*meso-* position) of styryl BODIPY. Therefore, the steric hindrance imposed by 1,7-methyl groups on the styryl BODIPY will restrict the rotation of PXZ, thus the dyads will adopt a perpendicular orientation between donor and acceptor. Styryl BODIPY shows strong red light-harvesting ability. The π-conjugated structure of **BDP-3** may lead to different triplet state properties, such as triplet state lifetime and triplet state energy. All molecular structures were fully characterized (refer to Experimental section and Supporting Information).

A single crystal of **BDP-1** was obtained by slow diffusion between *n*-hexane and DCM. The molecular structure determined by single crystal X-ray diffraction of **BDP-1** is presented in Figure 1. The dihedral angle between the electron donor (PXZ) and the acceptor (styryl BODIPY) is 71.4°, which is slightly different from the result of DFT calculation (89.7°), refer to later section. It also shows less orthogonality compared with the reported PTZ-styryl BODIPY dyad (−81.9°).[15] The possible reason is that the better planarity of PXZ compared to PTZ weakens the conformational restriction between the PXZ and styryl BODIPY moieties. The deviation from coplanar geometry of the styryl moieties is 10.9° and 28.4° due to the π-π stacking in the single crystal, because the DFT optimization of the ground state geometry indicated planar geometry. The structure of the styryl BODIPY moiety of **BDP-1** is more twisted than
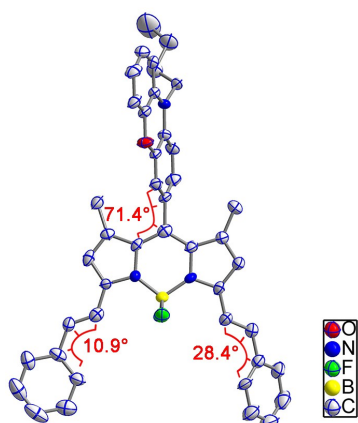
the reported PTZ-styryl BODIPY molecule (10.9° and 28.4° *vs* °4.7° and 1.2°).[15]

2.2. UV-Vis Absorption and Fluorescence Emission Spectra

The UV-Vis absorption spectra of the compounds were studied (Figure 2). The dyad **BDP-1** shows similar absorption compared with the reference **Styryl-BDP** in the region of 550–700 nm, which indicates negligible electronic coupling between the electron donor (PXZ) and the electron acceptor (styryl BODIPY) at the electronic ground state. A similar result was observed for **BDP-2**, the absorption is similar as that of **Styryl-BDP-CN**. However, the absorption band of **BDP-2** is slightly red-shifted compared to **BDP-1**. The UV-Vis absorption of **BDP-3** and **BDP-4** were also studied (Figure 2b). For **BDP-3**, a broad absorption band centered at 600 nm was observed, which shows the same absorption profile as the reference compound **BDP-4**. We conclude that the electronic coupling between donor and acceptor is also weak at the ground state of **BDP-3**. These features are similar to those observed for the BDP-PXZ dyads.[22]

Fluorescence spectra in different solvents were studied (Figure 3). For **BDP-1** (Figure 3a), structured emission bands centred at 630 nm and 685 nm were observed, which is similar to the unsubstituted compound **Styryl-BDP** (refer to the Supporting Information, Figure S11b). The fluorescence quantum yield (Φ_F) was determined as 73% in *n*-hexane (Table 1), which is similar to **Styryl-BDP** ($\Phi_F = 77\%$, Table 1). The results indicate that CT is inefficient in a non-polar solvent. However, the fluorescence is significantly quenched in more polar solvents. For instance, the Φ_F in toluene is almost half of that in *n*-hexane and it further decreased to 0.2% in acetonitrile (ACN) (Table 1). We attributed the fluorescence quenching to the electron transfer and formation of CT state, and the CT state is a dark state. Similar results were obtained for the dyad **BDP-2** (Figure 3b), but quenching of the fluorescence is more significant in polar solvents. For instance, the fluorescence quantum yield is 35.4% in *n*-hexane but it decreases to 0.5% in toluene (Table 1). In toluene, a broad and red-shifted emission band centred at 768 nm was observed, along with the LE emission band at 651 nm (Figure 4a). However, the emission at longer

Figure 1. Single-crystal structure of **BDP-1** with 50% thermal ellipsoids. Hydrogen atoms are omitted for clarity.
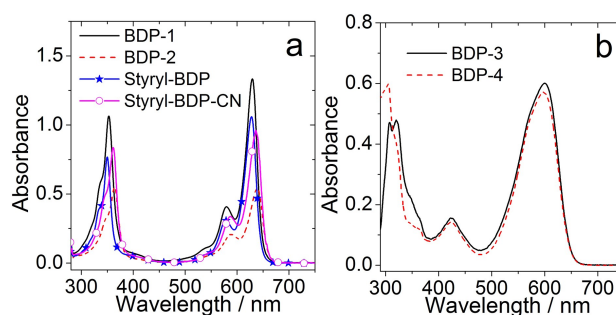

Figure 2. UV-Vis absorption spectra of compounds a) **BDP-1**, **BDP-2**, **Styryl-BDP** and **Styryl-BDP-CN**; b) **BDP-3** and **BDP-4**. $c = 1.0 \times 10^{-5}$ M in toluene. 20 °C.
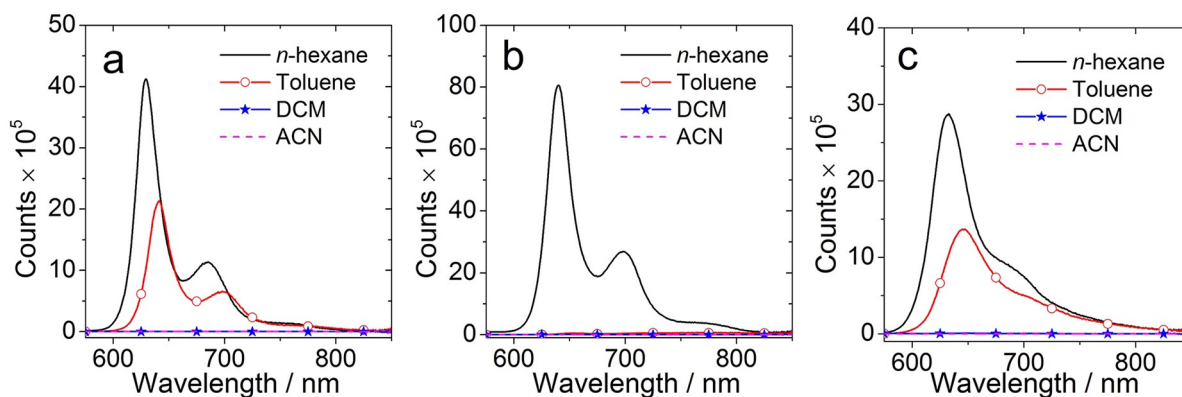
ChemPhysChem

Articles
doi.org/10.1002/cphc.202000300

**Chemistry
Europe**
European Chemical
Societies Publishing

Figure 3. Fluorescence emission spectra of the compounds in different solvents. a) **BDP-1**; b) **BDP-2**, and c) **BDP-3**. Optically matched solutions were used, i.e. all the sample solution show the same absorbance at the excitation wavelength ($A = 0.195$), $\lambda_{ex} = 570$ nm, 20 °C.

Table 1. The photophysical properties of compounds.

	Solvent[a]	λ_{abs}[b] (ε[c])	λ_F[d]	τ_F[e]	Φ_F[f]	Φ_Δ[g]	τ_T[h]	Φ_T[i]
BDP-1	HEX	620 (1.40)	629	5.4	0.732	_[l]	_[l]	_[l]
	TOL	630 (1.33)	641	4.9	0.393	0.23	333.2[k]	0.25
	ACN	619 (1.23)	631	2.9	0.002	_[l]	_[l]	_[l]
BDP-2	HEX	629 (0.57)	640	4.3	0.354	0.05	_[l]	_[l]
	TOL	639 (0.54)	651/768[j]	2.6/2.3[j]	0.005/0.018[j]	0.18	382.2[k]	0.22
	ACN	628 (0.53)	625	1.5	0.003	_[l]	_[l]	_[l]
BDP-3	HEX	597 (0.67)	633	3.0	0.484	0.04	394.4[k]	0.04
	TOL	600 (0.60)	647	2.4	0.299	0.12	392.7[k]	0.13
	ACN	590 (0.60)	629	1.4	0.003	_[l]	_[l]	_[l]
BDP-4	HEX	596 (0.66)	630	2.9	0.462	0.03	278.8[k]	0.05
	TOL	597 (0.57)	641	1.9	0.360	0.04	244.0	0.04
	ACN	587 (0.60)	631	0.07	0.022	_[l]	_[l]	_[l]
Styryl-BDP	HEX	619 (1.15)	630	5.2	0.768	_[l]	_[l]	_[l]
	TOL	628 (1.06)	641	4,7	0.768	_[l]	_[l]	_[l]
	ACN	617 (1.04)	631	5.2	0.763	_[l]	_[l]	_[l]
Styryl-BDP-CN	HEX	627 (0.78)	_[l]	_[l]	_[l]	_[l]	_[l]	_[l]
	TOL	636 (0.97)	649	4.2	0.652	_[l]	_[l]	_[l]
	ACN	627 (0.96)	639	4.4	0.612	_[l]	_[l]	_[l]

[a] $E_T(30)$ values are HEX (31.0), TOL (33.9) and ACN (45.6), in kcal mol^{-1}. [b] $c = 1.0 \times 10^{-5}$ M, in nm. [c] Molar absorption coefficient. $\varepsilon = 10^5$ M^{-1} cm^{-1}. [d] Fluorescence wavelength, in nm. [e] Fluorescence lifetime, $\lambda_{ex} = 635$ nm, in ns, $c = 1.0 \times 10^{-5}$ M. [f] Absolute fluorescence quantum yield. [g] Singlet oxygen quantum yield, methylene blue (**MB**) as standard ($\Phi_\Delta = 0.57$ in DCM). [h]Triplet state lifetime, in μs. [i] Triplet quantum yield, methylene blue (**MB**) as standard ($\Phi_T = 0.50$ in methanol). [j] The transition of ^{1}CT→S$_0$. [k] Intrinsic triplet state lifetimes. Obtained by fitting of the experimental curves based on the kinetic model with triplet-triplet-annihilation self-quenching effect considered.[22] [l] Not observed.
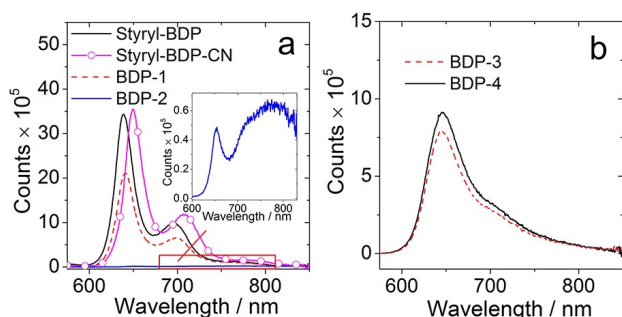

Figure 4. Comparison of the fluorescence emission spectra of the compounds in toluene: a) **BDP-1**, **BDP-2**, **Styryl-BDP** and **Styryl-BDP-CN**; b) **BDP-3** and **BDP-4**. Optically matched solutions were used ($A = 0.195$), $\lambda_{ex} = 570$ nm, 20 °C.

wavelength was quenched in polar solvent (Supporting Information, Figure S10b). Considering the relative fluorescence emission intensity and the quantum yields, the CT state of **BDP-2** is in principle also a dark state.

In toluene, the fluorescence is quenched both for **BDP-1** and **BDP-2** compared with the reference compounds **Styryl-BDP** and **Styryl-BDP-CN**. Furthermore, it is further quenched for **BDP-2** compared with **BDP-1** in toluene (Figure 3a). We attribute the significant quenching of the fluorescence of **BDP-2** as compared to **BDP-1** to the electron-withdrawing −CN groups, and the more significant CT in **BDP-2**. For **BDP-3**, the emission was quenched obviously in polar solvents, indicating an efficient CT. Compared with the reference compound **BDP-4**, the emission was slightly quenched in non-polar solvents such as *n*-hexane and toluene (Figure 4b and Table 1). However, the emission was quenched further in polar solvents, for instance,

Φ_F is 0.001 and 0.105 in DCM for **BDP-3** and **BDP-4**, respectively (Supporting Information, Table S2).

The fluorescence decay traces were studied using the time-correlated single-photon counting (TCSPC) detection method (Figure 5 and Supporting Information, Figure S12). The fluorescence lifetimes of **BDP-1** show solvent polarity dependency (Figure 4a). In non-polar solvents (*n*-hexane and toluene), the decay trace is mono-exponential. However, it shows a biexponential decay in polar solvents, such as ACN. The average lifetimes decrease from 5.4 ns (in *n*-hexane), to 2.9 ns (a short component of 0.06 ns with a population ratio of 30% and a longer component of 4.2 ns, in 70%) in ACN, meanwhile the fluorescence quantum yield decreased by 366-fold (Figure 3a and Table 1). Similar results are observed for **BDP-2** (Figure 5b and Table 1). The decay kinetics of **BDP-2** shows a sharper decrease along with increasing solvent polarity (Figure 5b). The lifetimes are also shorter than **BDP-1** in the same solvent (Table 1). For instance, the lifetime of **BDP-2** shows a bi-exponential decay with a short component of 0.12 ns (60%) and a longer component of 3.5 ns (40%). The fluorescence lifetime of **BDP-1** and **BDP-2** are 4.9 ns and 2.6 ns in toluene, respectively, which indicates that the CS of **BDP-2** is more efficient than that of **BDP-1**. We propose the bi-exponential decay is attributed to the existence of an equilibrium between the emissive state with a dark state (CT state), or electron transfer probability for the molecules at the ^{1}LE state, and the probability is less than unity.[6b] For **BDP-3**, a similar conclusion can be obtained (Supporting Information, Figure S12a). The
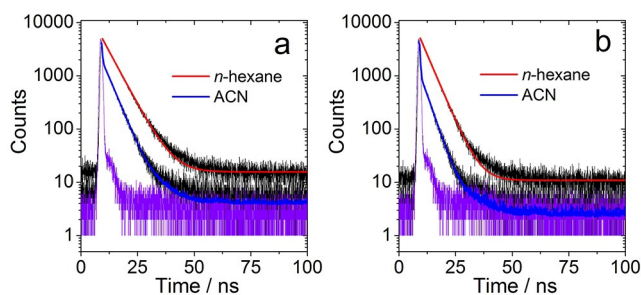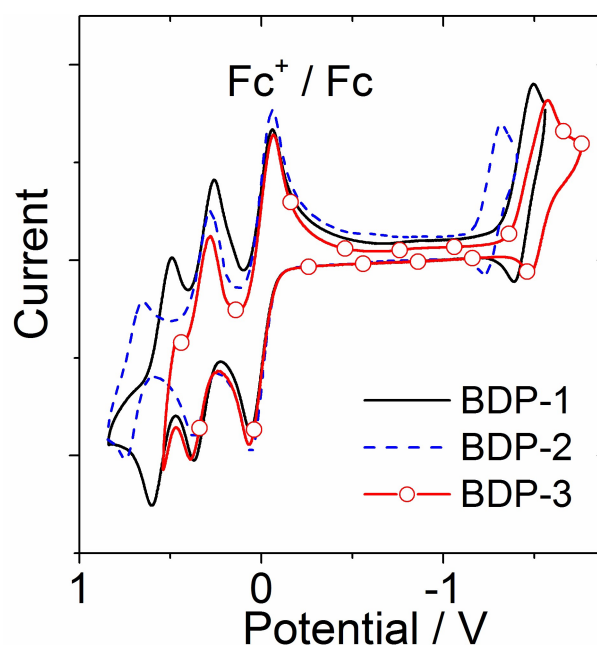

Figure 6. Cyclic voltammogram of **BDP-1**, **BDP-2** and **BDP-3**. Ferrocene (Fc) was used as internal reference. In deaerated DCM containing 0.10 M Bu$_4$N [PF$_6$] as supporting electrolyte. Scan rates: 100 mV/s. $c = 1.0 \times 10^{-3}$ M, 20 °C.

Figure 5. Fluorescence decay traces of the compounds in different solvents. a) **BDP-1** at 650 nm and b) **BDP-2** at 650 nm. $\lambda_{ex} = 635$ nm, $c = 1.0 \times 10^{-5}$ M. 20 °C. The IRF curves of the spectrometer are also presented.

fluorescence in *n*-hexane is mono-exponential with a lifetime of 3.0 ns. However, in ACN it turned to a bi-exponential decay with an average lifetime of 1.4 ns (with a short component of 0.10 ns (70%) and a longer component of 4.4 ns (30%)), indicating the fluorescence quenched further in polar solvents.

2.3. Electrochemical Studies

The electrochemical properties of the dyads were studied by cyclic voltammetry (Figure 6, Table 2, Supporting Information, Figure S22 and Table S4). For **BDP-1**, the reversible oxidation wave at +0.32 V (vs Fc/Fc$^+$) is attributed to the PXZ moiety, another quasi-reversible oxidation wave at +0.55 V is attributed to the styryl BODIPY moiety, as is the quasi-reversible reduction wave at −1.44 V. Therefore, PXZ is more likely the electron

Table 2. Redox potentials, driving forces of charge separation (ΔG_{CS}), charge recombination (ΔG_{CR}), and the energy of the CSS of the compounds (E_{CSS}) in different solvents.[a]

| | E(ox)[e] [V] | E(red)[e] [V] | ΔG_{CS} [eV][f] | | | | E_{CSS} [eV] | | | |
			HEX	TOL	DCM	ACN	HEX	TOL	DCM	ACN
BDP-1[b]	+0.55 +0.32	−1.44	0.09	−0.03	−0.36	−0.44	2.05	1.93	1.60	1.51
BDP-2[c]	+0.70 +0.33	−1.26	−0.004	−0.13	−0.47	−0.57	1.93	1.80	1.45	1.35
BDP-3[d]	+0.34	−1.52	−0.25	−0.29	−0.36	−0.38	1.73	1.70	1.62	1.59

[a] Cyclic voltammetry in N$_2$ saturated DCM containing a 0.10 M Bu$_4$NPF$_6$ supporting electrolyte; Pt electrode was used as counter electrode; working electrode is glassy carbon electrode; Ag/AgCl couple as the reference electrode. E_{00} is the energy difference between the potential minima, approximated with the crossing point of UV-Vis absorption and fluorescence emission spectra after normalization. [b] $E_{00} = 1.96$ eV. [c] $E_{00} = 1.92$ eV. [d] $E_{00} = 1.98$ eV. [e] The value was obtained by setting the oxidation potential of Fc$^+$/Fc as 0. [f] The redox potentials are approximated based on the redox potential measured in DCM.

ChemPhysChem

Articles
doi.org/10.1002/cphc.202000300

Chemistry
Europe
European Chemical
Societies Publishing

donor and styryl BODIPY serves as electron acceptor. The reduction wave of **BDP-2** was observed at −1.26 V, indicating the stronger electron accepting ability of the styryl BODIPY moiety with cyano groups attached, as compared with styryl BODIPY. Similar results were obtained for **BDP-3**. Only one reversible oxidation wave at +0.34 V and one quasi-reversible reduction wave at −1.52 V were observed, indicating that PXZ serves as electron donor and the BODIPY moiety serves as electron acceptor. Compared with the previously reported BDP-PXZ dyads, the oxidation potential of PXZ is similar (0.32 V vs 0.36 V, vs Fc/Fc$^+$).[6b] The reduction potentials of the styryl BODIPY moieties of **BDP-1** (−1.44 V) and **BDP-2** (−1.26 V) moves anodically than that of the BDP-PXZ dyad (−1.65 V, vs Fc/Fc$^+$), indicating the styryl BODIPY moieties are stronger electron acceptors than the parent BODIPY.

The Weller equations (Supporting Information, Equations S1–S4) were used to determine the energy of the charge separated state (CSS) and the driving forces of intramolecular charge separation (ΔG_{CS}).[8c] The results are summarized in Table 2 (For detailed information please refer to the Supporting Information).

The calculation of ΔG_{CS} indicates that charge separation is thermodynamically forbidden in *n*-hexane due to the positive ΔG_{CS} value (+0.09 eV) for **BDP-1**, which agrees with the unquenched fluorescence of styryl BODIPY moiety in *n*-hexane ($\Phi_F = 73.2\%$ in Table 1). However, thermodynamically allowed charge separation is possible in other more polar solvents according to the negative ΔG_{CS} values of **BDP-1**, which also

agrees with fluorescence quenching of the styryl BODIPY moiety (Table 1). For **BDP-2** and **BDP-3**, the ΔG_{CS} values are all negative, indicating charge separation is thermodynamically allowed in both nonpolar and polar solvents. For the previously reported BDP-PXZ dyads, the ΔG_{CS} values are all more negative.[22] For instance, the ΔG_{CS} values are −0.40 eV and −0.74 eV in toluene and ACN, respectively. For **BDP-1**, the ΔG_{CS} is −0.44 eV in ACN, indicating the CS driving force is weaker for **BDP-1**. It may reduce the CS and SOCT-ISC efficiency.

2.4. Femtosecond Transient Absorption Spectroscopy

Femtosecond transient absorption spectra (fs TA) were measured in order to reveal the excited state dynamics of the dyads. For **BDP-1**, the triplet state signal was observed in toluene (Figure 7), but no triplet state signal was observed in ACN. Hence we assume that the CS and CR are both much faster in ACN. In toluene, the intense ground state blenching (GSB) band at 630 nm was immediately generated upon excitation (Figure 7a). An excited state absorption (ESA) band in the range of 420–550 nm increased in intensity in less than 1 ps. This ESA band is attributed to the S$_1$→S$_n$ transition, and the increasing process may be due to vibrational relaxation. The negative band at 700 nm is assigned to stimulated emission (SE) of the localized singlet state (¹StyrylBDP*). However, no obvious absorption band of the PXZ radical cation (around 540 nm, Supporting Information, Figure S23b)[23] and the styryl BODIPY
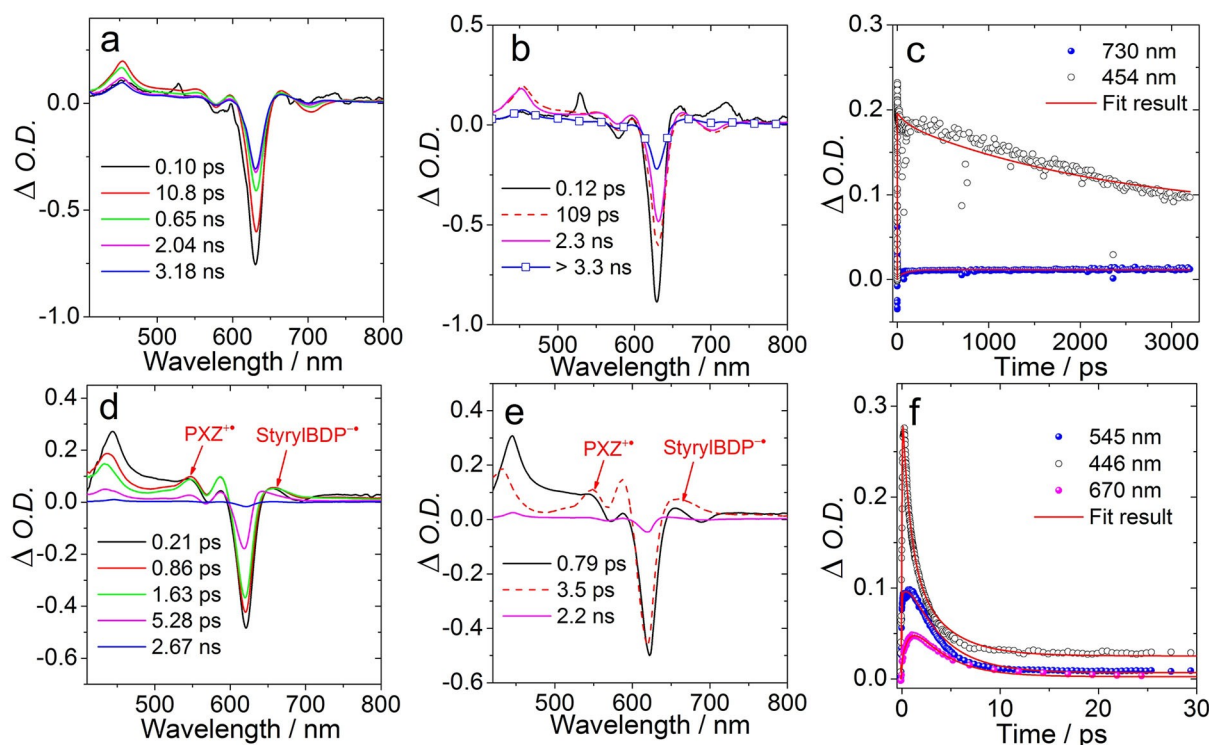

Figure 7. Femtosecond transient absorption spectra of **BDP-1**. a) Transient absorption spectra in toluene. $\lambda_{ex} = 630$ nm, $c = 1.0 \times 10^{-5}$ M, b) species-associated difference spectra (SADS), and c) decay traces at selected wavelengths. d) Transient absorption spectra of **BDP-1** in ACN ($\lambda_{ex} = 625$ nm, $c = 1 \times 10^{-5}$ M), e) species-associated difference spectra (SADS), and f) Decay traces at selected wavelengths. SADS were obtained by global fitting in sequential model. 20°C.

ChemPhysChem

Articles
doi.org/10.1002/cphc.202000300

Chemistry
Europe
European Chemical
Societies Publishing

radical anion (around 670 nm, Supporting Information, Figure S23a) were observed.

One possible reason is that the CS efficiency is not very high ($\Phi_F = 0.39$ in toluene). Furthermore, the radical anion absorption of styryl-BDP in the range of 650–680 nm (Supporting Information, Figure S23a and S23b, obtained by spectroelectrochemistry), overlaps with ESA signals of the singlet state of Styryl-BDP ('Figure 7a and Supporting Information, 'Figure S21). Moreover, the signal of the radical cation of PXZ also overlaps with the singlet state signal of styryl-BDP in the range of 530–550 nm ('Figure 7a and Supporting Information, 'Figure S21). Thus, we can't distinguish the characteristic ^{1}styryl-BDP* and the ^{1}CSS states unambiguously. The fs TA spectra of the reference compound **Styryl-BDP** were also recorded in toluene (Supporting Information, Figure S21). No fast decay of the GSB or the SE bands were observed, indicating that no CS exist in **Styryl-BDP**. Therefore, the CS is most likely responsible for the fast decay of **BDP-1** in toluene.

Species-associated difference spectra (SADS) obtained by global fitting were used to analyse the photophysical processes (Figure 7b). The species with the shortest lifetime (0.12 ps) is assigned to the unrelaxed S_1 state. The species with a lifetime of 109 ps displays the characteristic styryl BODIPY ESA signals (Supporting Information, 'Figure S21) and is assigned the relaxed S_1 state, indicating that CS process takes 109 ps. Subsequently, the slow CR takes 2.3 ns, and a long-lived species with infinite lifetime (on the time scale of the fs-TA experiment) is obtained, which is attributed to the triplet state. The final species is assigned as the T_1 state on account of showing a weak ESA band in the range 650-750 nm ($T_1 \rightarrow T_n$ absorption) and a GSB band at 630 nm, which is in agreement with ns TA data (Figure 8a). Therefore, we conclude that the triplet state is generated by the CR and the SOCT-ISC (CR) takes 2.3 ns.

In ACN, no triplet state signal was observed (Figure 7d). The ESA band located in the range of 440–570 nm is attributed to the $S_1 \rightarrow S_n$ absorption. Due to the higher CS efficiency, absorption bands of the styryl-BDP radical anion and the PXZ radical cation were more obvious. The absorption bands centered at 670 nm and 545 nm were attributed to styryl-BDP$^{-\bullet}$ and PXZ$^{+\bullet}$, respectively, which is in agreement with the results of spectroelectrochemical studies (refer to the Supporting Information, Figure S23a and S23b). Based on the SADS, we determined the time constants of the CS and CR as 0.79 ps and 3.5 ps, respectively (Figure 7e), which are faster than the CS (109 ps) and CR (2.2 ns) in toluene.

For **BDP-2**, the fluorescence was quenched significantly in toluene ($\Phi_F = 0.005$ vs. 0.393 of **BDP-1**). In toluene, a GSB band centered at 640 nm and a strong ESA band centered at 468 nm (Supporting Information, Figure S19a) were observed, which are assigned to the S_1 state. Subsequently, an absorption band at 670 nm intensified along with the decreasing ESA band at 469 nm, which is attributed to the formation of [StyrylBDP-CN]$^{-\bullet}$ (Supporting Information, Figure S23c). Finally, along with the decreasing of the absorption band centered at 670 nm, the ESA signal in the range of 650-750 nm become stronger, which is characteristic for the $T_1 \rightarrow T_n$ absorption of **BDP-2**, corroborated by the ns TA spectra (Supporting Information, Fig-
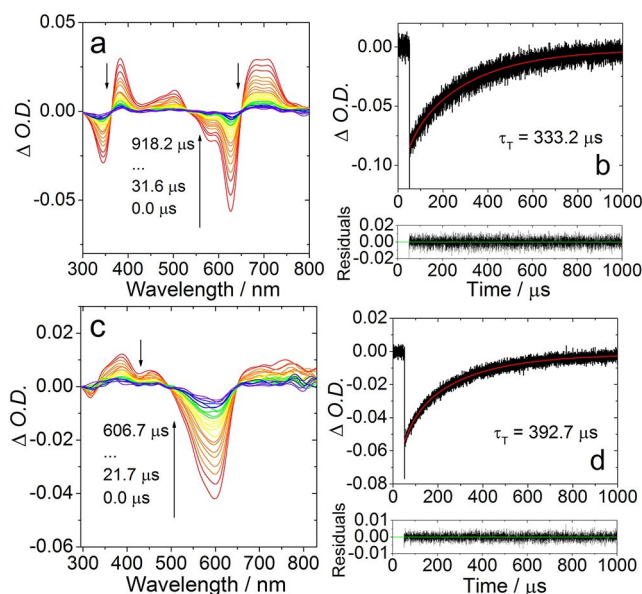

Figure 8. Nanosecond transient absorption spectra of compounds in de-aerated toluene. a) Transient absorption spectra of **BDP-1** at different delay time. b) The decay trace at 630 nm, $\lambda_{ex} = 620$ nm, $c = 5.0 \times 10^{-6}$ M. c) Transient absorption spectra of **BDP-3** and d) the decay trace at 600 nm, $\lambda_{ex} = 590$ nm, $c = 1.0 \times 10^{-5}$ M, 20 °C. The intrinsic lifetime was obtained by fitting of the decay curves with a kinetic model that takes into account of the triplet-triplet-annihilation effect.[22]

ure S13a). Therefore, we conclude that ISC occurs via CR. Based on the results from SADS (Supporting Information, Figure S19b), we determine that CS takes place in 1.2 ps, which is much faster than in **BDP-1** (109 ps in toluene). Following the CS, slow CR (SOCT-ISC) continuing for 1.6 ns leads to the generation of the triplet state of **BDP-2**. In the polar solvent ACN, results similar to those of **BDP-1** were obtained (Supporting Information, Figure S19e). Faster CS (0.3 ps) and CR (1.6 ps) are observed. No triplet state formation was observed, which agrees with the lack of singlet oxygen photosensitizing of the dyad **BDP-2** (Table 1).

Different results were obtained for **BDP-3** (Supporting Information, Figure S19). Upon excitation, the GSB band was observed in the range of 550–750 nm. It is broader than the UV-Vis absorption, which is attributed to the overlap of the GSB and the SE band. According to spectroelectrochemical results (Supporting Information, Figure S24), we determine the absorption of the radical anion and the radical cation centered at 580 nm and 540 nm, respectively. Based on the SADS analysis and the fast decay of ESA at 480 nm, we determine that CS takes 3.2 ps in toluene. The lifetime of the ^{1}CT state in toluene is ca. 4.0 ns. No triplet state formation was observed within the time resolution of our instrument setup.

2.5. Nanosecond Transient Absorption Spectroscopy: Triplet State Properties

Nanosecond transient absorption spectra were used to study the triplet state production of the dyads (Figure 8 and

ChemPhysChem

Articles
doi.org/10.1002/cphc.202000300

**Chemistry
Europe**
European Chemical
Societies Publishing

Supporting Information, Figure S13). For **BDP-1**, two negative peaks centered at 340 nm and 630 nm were observed upon pulsed laser excitation. In agreement with the UV-Vis absorption spectra (Figure 2a), these bands are assigned as GSB bands. Moreover, several ESA bands centred at 380 nm, 500 nm and 700 nm, respectively, were observed (Figure 8a). These features are typical of the styryl BODIPY triplet state transient absorption spectra.[24] Therefore, we conclude that the triplet state is localized on the styryl BODIPY moiety, and it is not a CT state. Similar results were obtained for **BDP-2** (In toluene, Supporting Information, Figure S13a). The GSB and ESA bands of **BDP-2** are both slightly red shifted compared with **BDP-1** due to the extension of π-conjugation structure. Recently with a PTZ-naphthalimide dyad, we observed a CT state.[16] Note the ESA bands overlap with the GSB bands.

The apparent triplet state lifetimes (τ_T) were determined as 270.0 µs for **BDP-1** and 242.7 µs for **BDP-2**, respectively, at a specific concentration. However, triplet-triplet annihilation (TTA) will quench the triplet state and shorten the triplet state lifetime, especially for the compounds showing strong absorption at the excitation wavelength, high ISC efficiency and long-lived triplet state. Therefore, the intrinsic triplet state lifetime was determined by fitting the decay traces at two different concentrations with a kinetic model including TTA self-quenching.[25] The intrinsic triplet state lifetime of **BDP-1** obtained with this kinetic model is $\tau_T = 333.2$ µs, which is much longer than the apparent triplet state lifetime $\tau_T = 270.0$ µs, indicating TTA quenching. For **BDP-2**, the intrinsic triplet state lifetime ($\tau_T = 382.2$ µs) is also longer than the experimental values (242.7 µs). Notably the triplet state lifetime of **BDP-1** is prolonged 185-fold ($\tau_T = 333.2$ µs) as compared to the triplet state of the same parent chromophore, i.e. bisstyryl-BODIPY, but accessed by the HAE in 2,6-diiodostyryl BODIPY (1.8 µs).[17] These results demonstrated one of the advantage of using the compact electron donor/acceptor dyads as heavy atom-free triplet PSs, i.e. the triplet state lifetime becomes much longer than that accessed with the conventional HAE.[15] Long-lived triplet state lifetime are important for photocatalysis, PDT and TTA-UC.

The ISC efficiency depends on the solvent polarity (Table 1). For instance, the triplet state quantum yield (Φ_T) for **BDP-1** is 25% in toluene (Table 1). However, in other solvents, no triplet state formation was observed. Similar results were observed for **BDP-2**. Therefore, we conclude that the ISC mechanism is based on charge recombination for **BDP-1** and **BDP-2**. Due to the short distance between electron donor/acceptor and strong electron coupling, SOCT-ISC is the most likely mechanism, instead of RP ISC. The poor SOCT-ISC in polar solvent may be due to the fast CR to the ground state (S_0 state), because the CR occurs normally in the Marcus inverted region, i.e. the lower CT state energy in polar solvent will accelerate CR to the S_0 state, thus inhibiting SOCT-ISC.[6b]

For **BDP-3**, the characteristic GSB and ESA signals are similar as the reference compound **BDP-4** (Figure 8c and Supporting Information, Figure S13c), which demonstrates that the triplet state is also localized on the BODIPY moiety. The intrinsic triplet state lifetime was determined as 392.7 µs in toluene (Table 1).

Theoretical computations were performed to study the ESA bands of $T_1 \rightarrow T_n$ transitions (Supporting Information, Figure S18). For **BDP-1**, the ESA bands centered at 700 nm, 500 nm and 375 nm are attributed to the $T_1 \rightarrow T_4$, $T_1 \rightarrow T_{10}$ and $T_1 \rightarrow T_{22}$ transitions, respectively (Supporting Information, Figure S18a). Similar results were obtained for **BDP-2**. The ESA band at 735 nm is attributed to the $T_1 \rightarrow T_4$ transition and the bands at 500 nm and 395 nm were assigned to the $T_1 \rightarrow T_{10}$ and $T_1 \rightarrow T_{22}$ transitions, respectively (Supporting Information, Figure S18b). The results of the calculations for **BDP-3** deviated from the experimental results (Supporting Information, Figure S18c). However, strong overlap between ESA and GSB bands can shift the apparent band maxima considerably. The ESA band at around 750 nm is assigned to the $T_1 \rightarrow T_{10}$ transition, the other two bands at around 460 nm and 380 nm were assigned to the $T_1 \rightarrow T_{12}$ and $T_1 \rightarrow T_{26}$ transitions, respectively.

Triplet-triplet energy transfer (TTET) was used to determine the triplet state energy of the dyads. **BDP-1** and **BDP-2** were used as triplet energy donors. Rubrene ($E_{T1} = 1.14$ eV)[26] and 1-chloro-9,10-bis(phenylethynyl)anthracene (CBPEA. $E_{T1} = 1.20$ eV)[4c] were selected as triplet energy acceptor. The triplet state lifetime of **BDP-1** wasn't quenched (260.2 µs) in the presence of 4 eq. CBPEA compared with that in the absence of CBPEA (272.3 µs) (Supporting Information, Figure S14b and S14d), which indicates the T_1 state energy of **BDP-1** is lower than that of CBPEA. In contrast, the triplet state lifetime of **BDP-1** was significantly quenched in the presence of 4 eq. rubrene (37.0 µs), indicating that the T_1 state energy of **BDP-1** is higher than 1.14 eV. Therefore, we estimate that the T_1 state energy of **BDP-1** is in the range of 1.14 ~ 1.20 eV. A similar result was obtained for **BDP-2** (Supporting Information, Figure S15), the T_1 state energy of **BDP-2** is in the range 1.14 ~ 1.20 eV. The results are also similar to those obtained by DFT calculation. The calculated T_1 state energies are 1.06 eV and 1.03 eV for **BDP-1** and **BDP-2**, respectively.

Due to the different π-conjugated structure of **BDP-3** compared with styryl BODIPY (Scheme 1), we assume the T_1 state energy of **BDP-3** is different from **BDP-1** and **BDP-2**. We selected BODIPY ($E_{T1} = 1.69$ eV)[27] and 9,10-diphenylanthracene (DPA) ($E_{T1} = 1.77$ eV)[28] as triplet energy acceptors and **BDP-3** as the energy donor. The triplet state lifetime of **BDP-3** decreased from 402.0 µs to 339.1 µs in the presence of BODIPY (Supporting Information, Figure S16). Meanwhile, a new GSB band appeared at around 500 nm, which is assigned to the GSB band of BODIPY. The decay at 500 nm is composed of two components, the increasing component is attributed TTET between **BDP-3** and BODIPY. These results demonstrate that the T_1 state energy of **BDP-3** is higher than 1.65 eV. On the contrary, no reduction of the triplet state lifetime of **BDP-3** was observed when DPA was used as the energy acceptor (Supporting Information, Figure S17). Therefore, we conclude that the T_1 state energy of **BDP-3** is in the range of 1.65 ~ 1.77 eV.

ChemPhysChem

Articles
doi.org/10.1002/cphc.202000300

Chemistry Europe
European Chemical
Societies Publishing

2.6. DFT Computations

The ground-state geometries of the dyads were optimized (Figure 9). The relative orientations between electron donor (PXZ) and acceptor (BODIPY chromophore) are all nearly orthogonal for all the dyads, which should be beneficial for SOCT-ISC. For instance, the dihedral angle between PXZ and styryl BODIPY in **BDP-1** is 89.7°, very close to orthogonal geometry. The π-conjugated structure of styryl BODIPY moiety of **BDP-1** shows minor distortion (by 1.8° and −1.7° at the two arms, respectively) (Figure 9a). These distortions are smaller than those observed in the single crystal structure (10.9° and 28.4°), the discrepancy may be due to the packing effect in the single crystal. The previously reported SOCT-ISC dyad BDP-PXZ has a similar dihedral angle between PXZ and BODIPY as found for **BDP-1** (85.6° vs 89.7°).[22]

For **BDP-2**, the relative orientations between the PXZ and the styryl BODIPY moieties are also orthogonal, and the distortions of the styryl moieties are 1.6° and −1.5° ('Figure 9). However, for **BDP-3**, the BODIPY chromophore moiety has better planarity (Supporting Information, Figure S25). The potential energy surfaces (PES) of the dyads against the torsional angles between electron donor and acceptor were also constructed (Supporting Information, Figure S26). For the three dyads, the thermally accessible dihedral angles between the electron donor and acceptor are all in the range of 65°∼113°. The range is similar (ca. 70°∼110°) for the reported PTZ-Styryl BODIPY dyads.[15]

The frontier molecular orbitals of the dyads are presented in Figure 10. For **BDP-1**, the lowest unoccupied molecular orbital (LUMO) is confined to the styryl BODIPY moiety, and the highest occupied molecular orbital (HOMO) is localized on the PXZ moiety, indicating that electron transfer is possible. Slight delocalization was observed. For **BDP-2**, the HOMO and LUMO are exclusively localized on the PXZ and styryl BODIPY moieties, respectively. For **BDP-3**, a similar result was observed. The MOs demonstrate that the attachment of electron withdrawing groups may alter the HOMO and LUMO energies. Compared
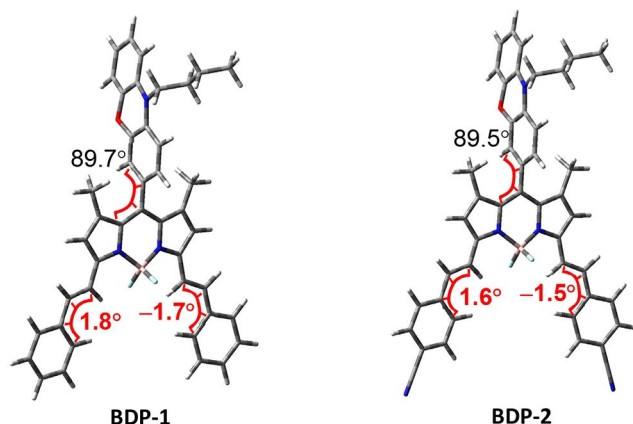
with **BDP-1**, the HOMO energy of **BDP-2** decreases from −4.90 eV to −5.02 eV and the LUMO energy shows a similar change (from −2.69 eV to −3.09 eV). The lack of overlap of the MO leads to more significant fluorescence quenching in **BDP-2**.

The triplet state spin density surfaces were studied at the optimized triplet state geometries (Figure 11). The spin un-paired electrons are localized on the styryl BODIPY moiety for **BDP-1** and **BDP-2**, which agrees with nanosecond transient absorption spectra (Figure 8). The spin density surfaces of the radical anion and the radical cation of **BDP-1** were also studied (Figure 12). The spin density of the radical anion is entirely restricted to the styryl BODIPY moiety. On the contrary, the spin density surface of the radical cation is completely localized on the PXZ moiety.

These results further imply that PXZ serves as electron donor and styryl BODIPY as the electron acceptor. Similar results were obtained for **BDP-2** and **BDP-3** (Supporting Information, Figure S29).

2.7. Application of the Dyads in TTA Upconversion

Recently, the application of heavy atom free triplet PSs on triplet-triplet annihilation upconversion (TTA-UC) has attracted particular interest.[29] Traditional heavy atom-free triplet PSs with absorption in the red range show low triplet energies, such as methylene blue (1.44 eV)[30] and 2,6-diiodostyryl BODIPY (ca. 1.13 eV).[31] Due to the low triplet state energy of **BDP-1** (1.14∼1.20 eV) and **BDP-2** (1.14∼1.20 eV), the dyad **BDP-3** was selected as the triplet PS of TTA-UC. The dyad **BDP-3** has high triplet state energy (1.65∼1.77 eV) and long intrinsic triplet state lifetime (392.7 μs in toluene), which is ideal for application for TTA-UC. TTA-UC was studied with **BDP-3** as PS and perylene as annihilator (Figure 13). Upon 589 nm cw laser excitation, only fluorescence of **BDP-3** was observed in absence of annihilator. A new emission peak appear in the region of 420–520 nm after addition of 4.0 eq. annihilator, which is attributed to the upconverted fluorescence of perylene (Figure 13a). The anti-Stokes shift of this TTA-UC system is 5905 cm^{-1}, and the upconversion quantum yield (Φ_{UC}) is 1.5% (in toluene). The anti-Stokes shift of **BDP-3** is comparable to the previously reported SOCT-ISC PSs applied in TTA-UC (ca. 3276–5900 cm^{-1}).[13a,22,32]

The power dependence of the upconversion emission intensity was measured (Supporting Information, Figure S31). The integrated upconversion emission intensity increased al-most linearly rather than quadratically with the excitation laser power, indicating efficient TTET and TTA for the TTA-UC system.

Finally, the intermolecular TTET was studied by Stern-Volmer analysis of the quenching by monitoring the triplet state lifetime of **BDP-3** (Supporting Information, Figure S32 and Table S5). The Stern-Volmer quenching constant ($K_{SV} = 1.74 \times 10^6$ M^{-1}) and quenching efficiency ($f_Q = 40.0\%$), indicating that intermolecular TTET is efficient.

The photophysical processes of **BDP-1** are summarized in Scheme 2. Upon excitation at 630 nm, the dyad is excited to the S_1 state (LE state localized on styryl BODIPY moiety). The

89.7°
1.8° −1.7°
BDP-1

89.5°
1.6° −1.5°
BDP-2

Figure 9. Optimized ground state geometry and selected dihedral angles of **BDP-1** and **BDP-2** calculated by DFT at the B3LYP/6-31G(d) level with Gaussian 09W.

ChemPhysChem

Articles
doi.org/10.1002/cphc.202000300

Chemistry Europe
European Chemical
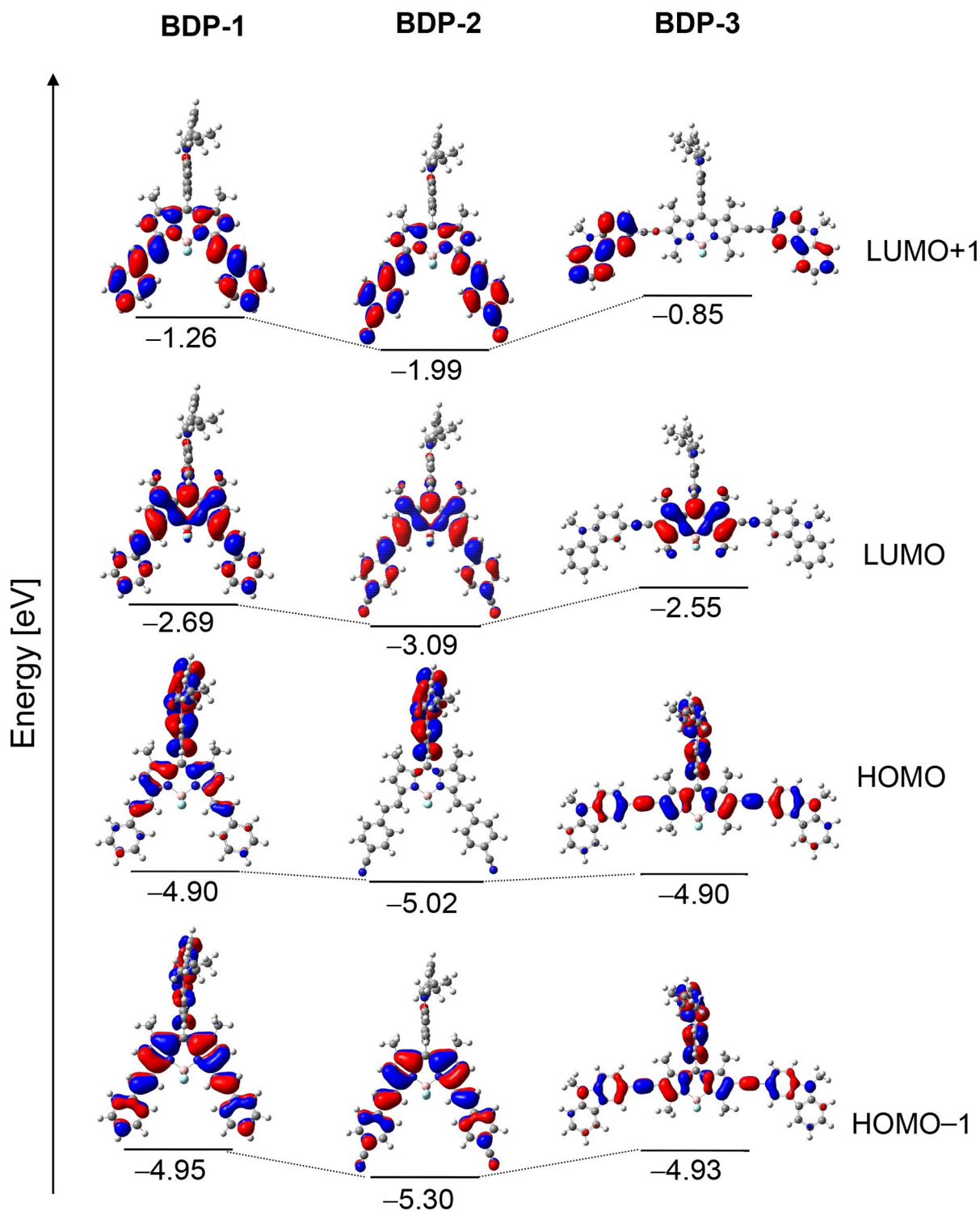Societies Publishing

Figure 10. Selected frontier molecular orbitals and energies (in eV) of the compounds calculated by DFT at the B3LYP/6-31G(d) level with Gaussian 09W, based on the optimized ground state structures. Isovalue = 0.02.

following CS leads to generation of a CS state, especially in polar solvents. ΔG_{CS} is positive and therefore CS is inhibited in *n*-hexane, resulting in unquenched fluorescence of the styryl BODIPY moiety (Table 1). In toluene, the fluorescence of the LE state is quenched by CS (rate constant 109 ps), subsequent CR

leads to population of T_1 (^{3}LE state). According to DFT calculations, SOCT-ISC to yield T_3 is also possible because the two states have similar energies,[10b] Ultrafast $T_3 \rightarrow T_1$ internal conversion will nevertheless populate T_1. The CR (ISC) rate constant was determined as 2.3 ns by femtosecond transient

ChemPhysChem

Articles
doi.org/10.1002/cphc.202000300

**Chemistry
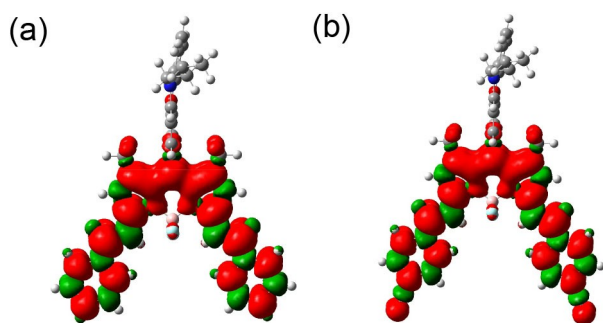Europe**
European Chemical
Societies Publishing

Figure 11. Isosurfaces of spin density of a) **BDP-1** and b) **BDP-2** at the optimized triplet state geometries. Calculation was performed at the UB3LYP/6-31G(d) level with Gaussian 09W. Isovalue = 0.0004.
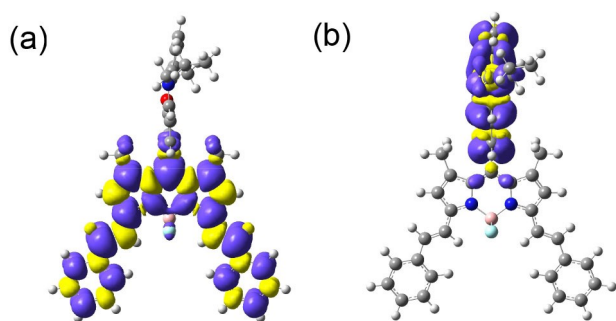

Figure 12. Isosurfaces of spin density of **BDP-1** at the optimized a) radical anion and b) radical cation geometries. Isovalue = 0.0004. The calculation was performed at the UB3LYP/6-31G(d) level with Gaussian 09W.

absorption spectra. The triplet quantum yield Φ_T is 25% in toluene. The energies of ^{1}CSS in more polar solvents are much lower (1.60 eV in DCM and 1.51 eV in ACN, respectively), which may facilitate the CR back to the ground state, because the CR is normally in Marcus inverted region of electron transfer.[6b] For instance, CR is much faster in ACN (3.5 ps) than in toluene (2.3 ns). Therefore, no triplet state signal was observed in DCM and ACN.

Similar photophysical processes are summarized for **BDP-2** (Supporting Information, Figure S33). CS occurs within 3.4 ps. The triplet state is confined to the styryl BODIPY moiety. It is produced by SOCT-ISC, with time constant of 1.4 ns (in toluene), and triplet state quantum yield $\Phi_T = 22$% (in toluene). For the dyad **BDP-3**, fast CS (3.2 ps) was observed, as well as a slow CR (4.0 ns). However, no triplet state signal was observed in femtosecond transient absorption spectra, due to the slow CR (SOCT-ISC) kinetics.

3. Conclusions

In summary, we prepared a series of phenoxazine-styryl BODIPY compact electron donor/acceptor dyads as novel heavy atom-free triplet photosensitizers (PSs), based on the newly developed spin-orbit charge transfer intersystem crossing (SOCT-ISC) strategy. The striking property of the new triplet PSs is the strong absorption of red light ($\varepsilon = 1.33 \times 10^5 \, M^{-1} \, cm^{-1}$ at 630 nm), and the long triplet state lifetime ($\tau_T = 333 \, \mu s$), prolonged by a factor of 180 compared to the triplet state of the same styryl BODIPY chromophore but accessed by the conventional heavy atom effect ($\tau_T = 1.8 \, \mu s$). Femtosecond transient absorption spectra show that the charge separation and SOCT-ISC (charge recombination) take 109 ps and 2.3 ns, respectively. The triplet state energies of the dyads **BDP-1** and **BDP-2** are 1.14~1.20 eV and **BDP-3** is 1.65~1.77 eV, determined by triplet energy transfer studies. The dyad **BDP-3** was used as triplet PSs for triplet-triplet annihilation upconversion (upconversion quantum yield $\Phi_T = 1.5$% in toluene; anti-Stokes shift is 5905 cm^{-1}). Our results are useful for the design of novel heavy atom-free triplet PSs showing red light-absorption and more importantly long-lived triplet states. These triplet PSs are useful for photo-redox catalytic organic reaction, photodynamic therapy, and triplet-triplet-annihilation photon upconversion.
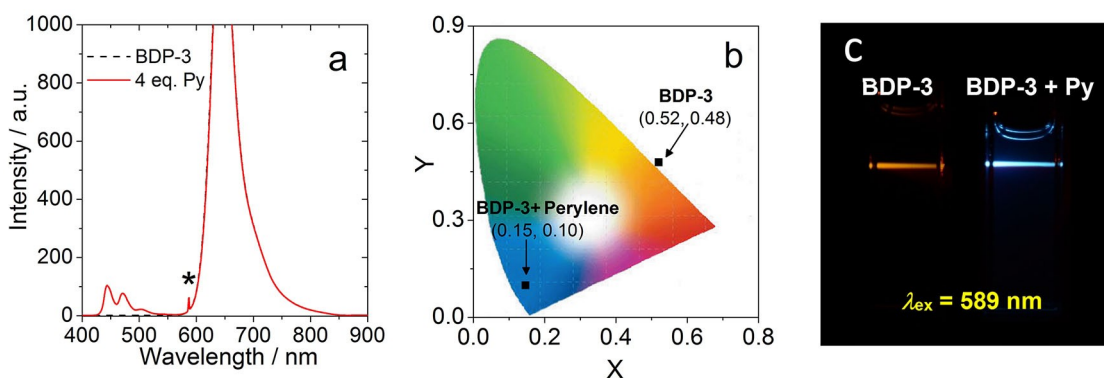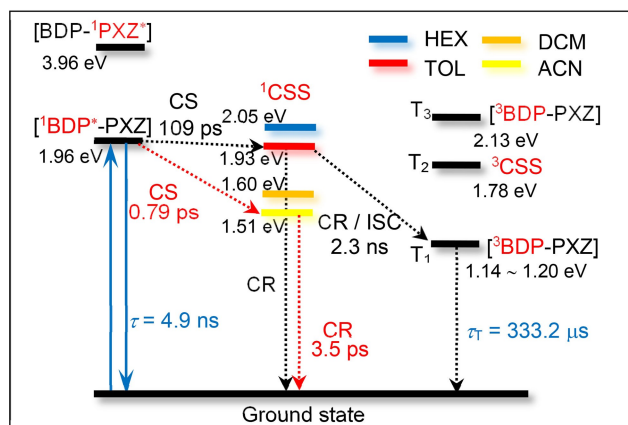

Figure 13. TTA upconversion with **BDP-3** as the triplet PS and perylene as the acceptor, $\lambda_{ex} = 589$ nm. $\Phi_{UC} = 1.5$%. a) Upconversion emission spectra. b) CIE diagram, and c) photographs of **BDP-3** alone and the upconversion. All spectra were measured upon excitation of the solution with the same 589 nm continuous wave laser (power density: 125 mW/cm^2). Data in diagrams (b) and (c) were measured with band-pass filter (transparent in the range 380-560 nm). c (**BDP-3**) = 1.0×10^{-5} M, c (perylene) = 4.0×10^{-5} M, in deaerated toluene, 20 °C.

ChemPhysChem

Articles
doi.org/10.1002/cphc.202000300

Chemistry Europe
European Chemical
Societies Publishing

Scheme 2. Photophysical processes of **BDP-1**. Energy of ^{1}CSS were obtained by the electrochemical characterization; Triplet state energies were obtained from TD-DFT calculation at the B3LYP/6-31G(d) level with Gaussian 09 W. Triplet state lifetime is the intrinsic lifetime, obtained by fitting of the decay traces with a kinetic model with the TTA effect considered.[22,25]

Experimental Section

Materials and Equipment

All compounds used for synthesis are analytically pure. Solvents for synthesis were freshly dried before using. ^{1}H and ^{13}C NMR spectra were recorded on Bruker 400/500 MHz spectrometers. HRMS (high resolution mass spectra) were recorded with MALDI-TOF-MS and ESI-MS spectrometers. Fluorescence spectra were recorded on a FS5 spectrofluorometer (Edinburgh Instrument Ltd, UK). UV-Vis spectra were recorded on a 8453 A UV-Vis spectrophotometer (Agilent Ltd, USA). The time-resolved emission spectra were recorded on a OB920 luminescence lifetime spectrometer (Edinburgh Instrument Ltd, UK).

Synthesis of BDP-1

Compound **3** (50 mg, 0.1 mmol), benzaldehyde (42.4 mg, 0.4 mmol), *p*-toluenesulfonic acid (PTSA) (15 mg, 0.08 mmol) and piperidine (0.5 mL) were dissolved in dry toluene (5 mL) and heated to 140 °C, then water generated during the reaction was removed from reaction mixture along with removal of toluene by distillation. The crude product was dissolved in DCM and washed with water. The organic layer was dried over anhydrous Na_2SO_4 and the solvent was removed with a rotary evaporator under reduced pressure. The crude product was purified by column chromatography (silica gel, PE/DCM = 1/1, v/v) to obtain **BDP-1** as dark blue solid (28 mg, yield: 42%). M.p. > 250 °C. ^{1}H NMR (400 MHz, CDCl$_3$): δ = 7.77–7.73 (dd, 2H), 7.86 (d, 4H, J = 8.0 Hz), 7.41 (t, 3H, J = 6.0 Hz), 7.35–7.29 (m, 3H), 7.25 (s, 1H), 2.55 (t, 2H, J = 6.0 Hz), 6.85 (t, 1H, J = 8.0 Hz), 6.72–6.65 (m, 5H), 6.57–6.53 (m, 3H), 3.55 (t, 2H, J = 8.0 Hz), 1.77 (s, 6H), 1.73–1.68 (m, 2H), 1.53–1.47 (m, 2H), 1.06 (t, 3H, J = 8.0 Hz). MALDI-TOF-HRMS: m/z [M]$^+$ Calcd for $C_{43}H_{38}BF_2N_3O^+$: m/z = 661.3076, found: m/z = 661.3055.

Synthesis of BDP-2

Compound **BDP-2** was prepared by a similar method used for **BDP-1**. Dark blue solid was obtained (4.5 mg, yield: 13%). M.p. > 250 °C. ^{1}H NMR (400 MHz, DMSO-d_6): δ = 8.38 (s, 2H), 8.23 (d, 2H, J = 8.0 Hz), 7.92–7.61 (m, 13H), 7.07 (s, 2H), 6.87–6.68 (m, 6H), 3.63 (s, 2H), 1.75

(s, 6H), 1.63–1.55 (m, 2H), 1.47–1.42 (m, 2H), 0.97 (t, 3H, J = 8.0 Hz). MALDI-TOF-HRMS: m/z [M]$^+$ Calcd for $C_{45}H_{36}BF_2N_5O^+$: m/z = 711.2981, found: m/z = 711.2998.

Synthesis of BDP-3

Under N_2 atmosphere, compound **4** (30 mg, 0.04 mmol) and **7** (80 mg, 0.32 mmol) was dissolved in mixed solvent TEA/THF (10 mL, 1:1, v/v). Then PdCl$_2$(PPh$_3$)$_2$ (7 mg), PPh$_3$ (5 mg) and CuI (3.8 mg) were added and the reaction was heated to 60 °C for 3 h. The product was washed with water after cooling to room temperature. The organic layer was collected and dried over anhydrous Na_2SO_4. The crude product was purified by column chromatography (silica gel, PE/DCM = 2/1, v/v) to obtain **BDP-3** as dark violet solid (24 mg, yield: 60%). M.p. > 250 °C. ^{1}H NMR (400 MHz, DMSO-d_6): δ = 8.38 (s, 2H), 8.23 (d, 2H, J = 8.0 Hz), 7.66–7.58 (m, 6H), 7.51–7.48 (m, 2H), 7.25–7.22 (m, 2H), 6.92 (s, 3H), 6.79–6.71 (m, 4H), 4.42 (t, 4H, J = 8.0 Hz), 3.65 (t, 2H, J = 6.0 Hz), 2.69 (s, 6H), 1.86 (s, 6H), 1.76 (t, 4H, J = 6.0 Hz), 1.62 (t, 2H, J = 6.0 Hz), 1.50–1.44 (m, 2H), 1.33–1.27 (m, 4H), 0.99 (t, 3H, J = 6.0 Hz), 0.88 (t, 6H, J = 8.0 Hz). MALDI-TOF-HRMS: m/z [M]$^+$ Calcd for $C_{65}H_{60}BF_2N_5O^+$: m/z = 975.4859, found: m/z = 975.4841.

Femtosecond Transient Absorption Spectra

The femtosecond transient absorption spectra were performed on a Ti:sapphire laser amplifier-optical parametric amplifier system with 52 fs pulse duration and 1 kHz repetition rate (Spectra-Physics, Spitfire Pro XP, TOPAS) and a commercial setup of an ultrafast transient absorption spectrometer (Spectra Physics, Helios). The excitation wavelength was determined by steady UV-Vis absorption spectra. Perpendicular angle between the probe and the pump beam polarization direction was used. The Surface Xplorer and Glotaran software were used for processing the experimental data after chirp correction.

Nanosecond Transient Absorption Spectra

Nanosecond transient absorption spectra were recorded on a LP980 laser flash photolysis spectrometer (Edinburgh Instruments, Ltd UK). All the sample solutions are deaerated with N_2 for *ca.* 15 min before measuring. The samples were excited with a nanosecond pulsed laser (Opolette^{TM}, the wavelength is tunable in the range of 210–2400 nm. OPOTEK, USA). The typical laser power is 5 mJ per pulse. The signal was digitized on a Tektronix TDS 3012B oscilloscope. The data were analyzed with the L900 software. The intrinsic triplet state lifetime was obtained by fitting of the decay traces of the compounds at different concentrations with a kinetic model that takes into account of the triplet-triplet-annihilation quenching effect.[22]

Single Crystal X-Ray Crystallography

X-ray diffraction data were collected on a Bruker SMART APEX-II CCD diffractometer (Mo Kα radiation, λ = 0.71073 Å) at 200 K using the SMART and SAINT programs. The structure was solved by direct method of SHELXTL-97 and refined by full-matrix least-squares using the SHELXL-2014 program on a PC. H atoms were generated geometrically. Detailed crystallographic data and structure refinement parameters are available in the Supporting Information, Table S1. The crystallographic data for the structure can be obtained from the Cambridge Crystallographic Data Centre via www.ccdc.cam.ac.uk with CCDC number: 1990853.

ChemPhysChem

Articles
doi.org/10.1002/cphc.202000300

Chemistry Europe
European Chemical
Societies Publishing

Triplet State Quantum Yield (Φ_T)

The triplet state quantum yields were determined by the ground state bleaching method based on the data measured by nanosecond transient absorption spectra using the following equation:

$$\Phi_{sam} = \Phi_{std} \left(\frac{\varepsilon_{std}}{\varepsilon_{sam}} \right) \left(\frac{\Delta A_{sam}}{\Delta A_{std}} \right)$$

In the equation, "sam" and "std" represent sample and standard, respectively. Φ is the triplet state quantum yield, ε is the molar absorption coefficient determined by UV-Vis absorption spectra, ΔA is the optical intensity of the GSB band determined by nanosecond transient absorption spectra. Optically matched solutions were used (the absorbance of sample and standard solutions is the same at the excitation wavelength) for the measurement of determination of ΔA. Methylene blue (MB) as standard ($\Phi_T = 0.50$ in methanol).

DFT Calculation

All DFT calculations were performed by using the Gaussian 09 program package.[33] The ground state geometries, spin density calculations of triplet state and radical anion/cation were optimized by using density functional theory (DFT) at the B3LYP/6-31G(d) level. The spin density calculations of triplet state were performed by setting the charge as 0 and spin as triplet. The spin density calculations of radical anion and cation were performed by setting the charge as -1 and $+1$, respectively and spin was set as doublet automatically. The frontier molecular orbitals and the energy levels of the compounds calculated by TD-DFT at the B3LYP/6-31G(d) level.

Acknowledgements

Conflict of Interest

The authors declare no conflict of interest.

Keywords: BODIPY · charge transfer · intersystem crossing · photosensitizers · triplet state

[1] a) Y. Wu, W. Zhu, *Chem. Soc. Rev.* **2013**, *42*, 2039–2058; b) A. Maldotti, A. Molinari, R. Amadelli, *Chem. Rev.* **2002**, *102*, 3811–3836; c) N. Zhang, S. R. Samanta, B. M. Rosen, V. Percec, *Chem. Rev.* **2014**, *114*, 5848–5958.

[2] a) J. P. Celli, B. Q. Spring, I. Rizvi, C. L. Evans, K. S. Samkoe, S. Verma, B. W. Pogue, T. Hasan, *Chem. Rev.* **2010**, *110*, 2795–2838; b) S. G. Awuah, Y. You, *RSC Adv.* **2012**, *2*, 11169–11183; c) A. Kamkaew, S. H. Lim, H. B. Lee, L. V. Kiew, L. Y. Chung, K. Burgess, *Chem. Soc. Rev.* **2013**, *42*, 77–88; d) G. Zerbi, A. Barbon, R. Bengalli, A. Lucotti, T. Catelani, F. Tampieri, M. Gualtieri, M. D'Arienzo, F. Morazzoni, M. Camatini, *Nanoscale* **2017**, *9*, 13640–13650; e) M. L. Agazzi, J. E. Durantini, N. S. Gsponer, A. M. Durantini, S. G. Bertolotti, E. N. Durantini, *ChemPhysChem*, **2019**, *20*, 1110–1125; f) M. B. Ballatore, M. E. Milanesio, H. Fujita, J. S. Lindsey, E. N.

Durantini, *J. Biophotonics.* **2020**, 13:e201960061; g) A. C. Scanone, S. C. Santamarina, D. A. Heredia, E. N. Durantini, A. M. Durantini, *ACS Applied Bio Materials* **2020**, *3*, 1061–1070; h) V.-N. Nguyen, S. Qi, S. Kim, N. Kwon, G. Kim, Y. Yim, S. Park, J. Yoon, *J. Am. Chem. Soc.* **2019**, *141*, 16243–16248; i) V.-N. Nguyen, Y. Yim, S. Kim, B. Ryu, K. M. K. Swamy, G. Kim, N. Kwon, C.-Y. Kim, S. Park, J. Yoon, *Angew. Chem. Int. Ed.* 10.1002/anie.202002843.

[3] a) J. Bartelmess, W. W. Weare, R. D. Sommer, *Dalton Trans.* **2013**, *42*, 14883–14891; b) E. Giannoudis, E. Benazzi, J. Karlsson, G. Copley, S. Panagiotakis, G. Landrou, P. Angaridis, V. Nikolaou, C. Matthaiaki, G. Charalambidis, E. A. Gibson, A. G. Coutsolelos, *Inorg. Chem.* **2020**, *59*, 1611–1621; c) P. Wang, S. Guo, S.-J. Wang, K.-K. Chen, N. Zhang, Z.-M. Zhang, T.-B. Lu, *Nat. Commun.* **2019**, *10*, 3155.

[4] a) J. Zhao, W. Wu, J. Sun, S. Guo, *Chem. Soc. Rev.* **2013**, *42*, 5323–5351; b) J. Zhou, Q. Liu, W. Feng, Y. Sun, F. Li, *Chem. Rev.* **2015**, *115*, 395–465; c) W. Wu, H. Guo, W. Wu, S. Ji, J. Zhao, *J. Org. Chem.* **2011**, *76*, 7056–7064; d) S. Shokri, G. P. Wiederrecht, D. J. Gosztola, A. J.-L. Ayitou, *J. Phys. Chem. C* **2017**, *121*, 23377–23382; e) T. N. Singh-Rachford, F. N. Castellano, *Coord. Chem. Rev.*, **2010**, *254*, 2560–2573.

[5] a) W.-Y. Wong, C.-L. Ho, *Acc. Chem. Res.* **2010**, *43*, 1246–1256; b) J. Lee, P. Jadhav, P. D. Reusswig, S. R. Yost, N. J. Thompson, D. N. Congreve, E. Hontz, T. Van Voorhis, M. A. Baldo, *Acc. Chem. Res.* **2013**, *46*, 1300–1311; c) E. Castellucci, M. Monini, M. Bessi, A. Iagatti, L. Bussotti, A. Sinicropi, M. Calamante, L. Zani, R. Basosi, G. Reginato, A. Mordini, P. Foggi, M. Di Donato, *Phys. Chem. Chem. Phys.*, **2017**, *19*, 15310–15323.

[6] a) T. Yogo, Y. Urano, Y. Ishitsuka, F. Maniwa, T. Nagano, *J. Am. Chem. Soc.* **2005**, *127*, 12162–12163; b) N. J. Turro, V. Ramamurthy, J. C. Scaiano, *Principles of Molecular Photochemistry: An Introduction*, University Science Books: Sausalito, California, **2009**; c) P.-T. Chou, Y. Chi, M.-W. Chung, C.-C. Lin, *Coord. Chem. Rev.* **2011**, *255*, 2653–2665.

[7] a) W. Wu, W. Wu, S. Ji, H. Guo, P. Song, K. Han, L. Chi, J. Shao, J. Zhao, *J. Mater. Chem.* **2010**, *20*, 9775–9786; b) R. Lincoln, L. Kohler, S. Monro, H. Yin, M. Stephenson, R. Zong, A. Chouai, C. Dorsey, R. Hennigar, R. P. Thummel, S. A. McFarland, *J. Am. Chem. Soc.* **2013**, *135*, 17161–17175.

[8] a) H. Levanon, J. R. Norris, *Chem. Rev.* **1978**, *78*, 185–198; b) J. W. Verhoeven, *J. Photochem. Photobiol. C* **2006**, *7*, 40–60; c) R. Ziessel, B. D. Allen, D. B. Rewinska, A. Harriman, *Chem.–Eur. J.* **2009**, *15*, 7382–7393; d) M. A. Collini, M. B. Thomas, V. Bandi, P. A. Karr, F. D'Souza, *Chem. Eur. J.* **2017**, *23*, 4450–4461; e) G. P. Wiederrecht, W. A. Svec, M. R. Wasielewski, T. Galili, H. Levanon, *J. Am. Chem. Soc.* **2000**, *122*, 9715–9722.

[9] a) D. I. Schuster, P. Cheng, P. D. Jarowski, D. M. Guldi, C. Luo, L. Echegoyen, S. Pyo, A. R. Holzwarth, S. E. Braslavsky, R. M. Williams, G. Klihm, *J. Am. Chem. Soc.* **2004**, *126*, 7257–7270; b) Z. E. X. Dance, Q. Mi, D. W. McCamant, M. J. Ahrens, M. A. Ratner, M. R. Wasielewski, *J. Phys. Chem. B* **2006**, *110*, 25163–25173.

[10] a) H. van Willigen, G. Jones, M. S. Farahat, *J. Phys. Chem.* **1996**, *100*, 3312–3316; b) Z. E. X. Dance, S. M. Mickley, T. M. Wilson, A. B. Ricks, A. M. Scott, M. A. Ratner, M. R. Wasielewski, *J. Phys. Chem. A* **2008**, *112*, 4194–4201; c) M. A. Filatov, S. Karuthedath, P. M. Polestshuk, H. Savoie, K. J. Flanagan, C. Sy, E. Sitte, M. Telitchko, F. Laquai, R. W. Boyle, M. O. Senge, *J. Am. Chem. Soc.* **2017**, *139*, 6282–6285; d) X.-F. Zhang, N. Feng, *Chem. Asian J.* **2017**, *12*, 2447–2456; e) M. A. Filatov, *Org. Biomol. Chem.* **2020**, *18*, 10–27; f) W. Hu, M. Liu, X.-F. Zhang, Y. Wang, Y. Wang, H. Lan, H. Zhao, *J. Phys. Chem. C* **2019**, *123*, 15944–15955; g) X.-F. Zhang, N. Feng, *Spectrochim. Acta Part A* **2018**, *189*, 13–21; h) S. Das, W. G. Thornbury, A. N. Bartynski, M. E. Thompson, S. E. Bradforth, *J. Phys. Chem. Lett.*, **2018**, *9*, 3264–3270; i) Y. Hou, T. Biskup, S. Rein, Z. Wang, L. Bussotti, N. Russo, P. Foggi, J. Zhao, G. Mazzone, S. Weber, *J. Phys. Chem. C*, **2018**, *122*, 27850–27865.

[11] W. M. Kwok, C. Ma, P. Matousek, A. W. Parker, D. Phillips, W. T. Toner, M. Towrie, P. Zuo, D. L. Phillips, *Phys. Chem. Chem. Phys.* **2003**, *5*, 3643–3652.

[12] M. Imran, A. A. Sukhanov, Z. Wang, A. Karatay, J. Zhao, Z. Mahmood, A. Elmali, V. K. Voronkova, M. Hayvali, Y. H. Xing, S. Weber, *J. Phys. Chem. C* **2019**, *123*, 7010–7024.

[13] a) Z. Wang, J. Zhao, *Org. Lett.* **2017**, *19*, 4492–4495; b) M. A. Filatov, S. Karuthedath, P. M. Polestshuk, S. Callaghan, K. J. Flanagan, M. Telitchko, T. Wiesner, F. Laquai, M. O. Senge, *Phys. Chem. Chem. Phys.* **2018**, *20*, 8016–8031.

[14] a) D. Veldman, S. M. A. Chopin, S. C. J. Meskers, R. A. J. Janssen, *J. Phys. Chem. A* **2008**, *112*, 8617–8632; b) Y. Zhao, R. Duan, J. Zhao, C. Li, *Chem. Commun.* **2018**, *54*, 12329–12332.

[15] Y. Hou, Q. Liu, J. Zhao, *Chem. Commun.* **2020**, *56*, 1721–1724.

[16] a) G. Tang, A. A. Sukhanov, J. Zhao, W. Yang, Z. Wang, Q.-Y. Liu, V. K. Voronkova, M. Di Donato, D. Escudero, D. Jacquemin, *J. Phys. Chem. C*,

ChemPhysChem

Articles
doi.org/10.1002/cphc.202000300

Chemistry
Europe
European Chemical
Societies Publishing

2019, *123*, 30171–30186; b) D. Liu, A. M. El-Zohry, M. Taddei, C. Matt, L. Bussotti, Z. Wang, J. Zhao, O. F. Mohammed, M. Di Donato, S. Weber, *Angew. Chem. Int. Ed.* 10.1002/anie.202003560.

[17] L. Huang, J. Zhao, S. Guo, C. Zhang, J. Ma, *J. Org. Chem.* **2013**, *78*, 5627–5637.

[18] a) A. Gorman, J. Killoran, C. O'Shea, T. Kenna, W. M. Gallagher, D. F. O'Shea, *J. Am. Chem. Soc.* **2004**, *126*, 10619–10631; b) N. Adarsh, R. R. Avirah, D. Ramaiah, *Org. Lett.* **2010**, *12*, 5720–5723; c) S. Guo, L. Ma, J. Zhao, B. Küçüköz, A. Karatay, M. Hayvali, H. G. Yaglioglu, A. Elmali, *Chem. Sci.* **2014**, *5*, 489–500.

[19] J. Zhao, S. Ji, H. Guo, *RSC Adv.* **2011**, *1*, 937–950.

[20] a) Z. Shi, J. Li, Q. Han, X. Shi, C. Si, G. Niu, P. Ma, M. Li, *Inorg. Chem.* **2019**, *58*, 12529–12533; b) S. Ghosh, C. K. Jana, *Org. Biomol. Chem.* **2019**, *17*, 10153–10157.

[21] a) H. Tanaka, K. Shizu, H. Miyazaki, C. Adachi, *Chem. Commun.* **2012**, *48*, 11392–11394; b) Q. Zhang, B. Li, S. Huang, H. Nomura, H. Tanaka, C. Adachi, *Nat. Photonics* **2014**, *8*, 326–332.

[22] Y. Dong, A. A. Sukhanov, J. Zhao, A. Elmali, X. Li, B. Dick, A. Karatay, V. K. Voronkova, *J. Phys. Chem. C* **2019**, *123*, 22793–22811.

[23] T. Akasaka, A. Nakata, M. Rudolf, W.-W. Wang, M. Yamada, M. Suzuki, Y. Maeda, R. Aoyama, T. Tsuchiya, S. Nagase, D. M. Guldi, *ChemPlusChem* **2017**, *82*, 1067–1072.

[24] L. Huang, X. Yu, W. Wu, J. Zhao, *Org. Lett.* **2012**, *14*, 2594–2597.

[25] a) Z. Lou, Y. Hou, K. Chen, J. Zhao, S. Ji, F. Zhong, Y. Dede, B. Dick, *J. Phys. Chem. C* **2018**, *122*, 185–193; b) Z. Wang, A. A. Sukhanov, A. Toffoletti, F. Sadiq, J. Zhao, A. Barbon, V. K. Voronkova, B. Dick J Phys, *Chem. C* **2019**, *123*, 265–274.

[26] W. G. Herkstroeter, P. B. Merkel, *J. Photochem.* **1981**, *16*, 331–342.

[27] A. A. Rachford, R. Ziessel, T. Bura, P. Retailleau, F. N. Castellano, *Inorg. Chem.* **2010**, *49*, 3730–3736.

[28] M. Montalti, A. Credi, L. Prodi, M. T. Gandolfi, *Handbook of photo-chemistry*, CRC press, **2006**.

[29] a) W. Wu, X. Cui, J. Zhao, *Chem. Commun.* **2013**, *49*, 9009–9011; b) J. Peng, X. Guo, X. Jiang, D. Zhao, Y. Ma, *Chem. Sci.* **2016**, *7*, 1233–1237.

[30] D. R. Kearns, R. A. Hollins, A. U. Khan, R. W. Chambers, P. Radlick, *J. Am. Chem. Soc.* **1967**, *89*, 5455–5456.

[31] J. Ma, X. Yuan, B. Kucukoz, S. Li, C. Zhang, P. Majumdar, A. Karatay, X. Li, H. G. Yaglioglu, A. Elmali, J. Zhao, M. Hayvali, *J. Mater. Chem. C* **2014**, *2*, 3900–3913.

[32] Z. Wang, J. Zhao, M. Di Donato, G. Mazzone, *Chem. Commun.* **2019**, *55*, 1510–1513.

[33] Gaussian 09, Revision 09 W, M. J. Frisch, G. W. Trucks, H. B. Schlegel, G. E. Scuseria, M. A. Robb, J. R. Cheeseman, G. Scalmani, V. Barone, B. Mennucci, G. A. Petersson, H. Nakatsuji, M. Caricato, X. Li, H. P. Hratchian, A. F. Izmaylov, J. Bloino, G. Zheng, J. L. Sonnenberg, M. Hada, M. Ehara, K. Toyota, R. Fukuda, J. Hasegawa, M. Ishida, T. Nakajima, Y. Honda, O. Kitao, H. Nakai, T. Vreven, J. A. Montgomery, Jr., J. E. Peralta, F. Ogliaro, M. Bearpark, J. J. Heyd, E. Brothers, K. N. Kudin, V. N. Staroverov, R. Kobayashi, J. Normand, K. Raghavachari, A. Rendell, J. C. Burant, S. S. Iyengar, J. Tomasi, M. Cossi, N. Rega, J. M. Millam, M. Klene, J. E. Knox, J. B. Cross, V. Bakken, C. Adamo, J. Jaramillo, R. Gomperts, R. E. Stratmann, O. Yazyev, A. J. Austin, R. Cammi, C. Pomelli, J. W. Ochterski, R. L. Martin, K. Morokuma, V. G. Zakrzewski, G. A. Voth, P. Salvador, J. J. Dannenberg, S. Dapprich, A. D. Daniels, Ö. Farkas, J. B. Foresman, J. V. Ortiz, J. Cioslowski, D. J. Fox, Gaussian, Inc. Wallingford CT, **2009**.